JOURNAL OF PROPULSION AND POWER
Vol. 23, No. 3, May–June 2007

Thickness of Liquid Film Formed by Impinging Jets on a Concave Wall

Takao Inamura,* Shin Amagasaki,† and Hideki Yanaoka‡
Hirosaki University, Hirosaki 036-8561, Japan

DOI: 10.2514/1.27691

The theoretical analysis of the liquid flow flowing over the flat solid wall derived in a previous paper is extended to the film flow on the concave wall. In addition, the equations used to predict the liquid film thickness on the concave wall are derived. The measurements of the film thickness on the concave wall are performed by the contact needle method, while varying the impingement angle, the curvature of the concave wall, the distance between the measurement point and the impingement point, and the jet Reynolds number. The predictions of the film thickness distribution are compared with the measurements. The comparisons show that the predictions of the film thickness agree well with the measurements, except in the region near the symmetry axis of the liquid film. In the region near the symmetry axis, the predictions overestimate the film thickness. The discrepancies appear to be a result of the assumptions in the theoretical analysis with respect to the film flow near the impingement point.

Nomenclature

A	=	constant
a	=	radius of the impinging liquid jet
B	=	constant
D	=	diameter of the liquid injection nozzle
G	=	Goertler number
h	=	liquid film thickness
Q	=	liquid volume flow rate, $\pi a^2 U_0$
R	=	radius of the concave wall
Re	=	jet Reynolds number
U	=	velocity of the liquid film surface
U_0	=	liquid jet velocity
u	=	velocity of liquid in the radial direction
w	=	distance between the centerline of the liquid jet and the streamline passing through the stagnation point
X	=	coordinate system
x	=	coordinate system
Y	=	coordinate system
y	=	coordinate system
z	=	coordinate perpendicular to the solid wall
α	=	coordinate in the azimuthal direction in a cross section of the liquid jet
δ	=	boundary-layer thickness
δ_2	=	momentum thickness
η	=	nondimensional coordinate, z/h_ϕ
θ	=	impingement angle
θ_N	=	angle along the concave wall surface
ν	=	kinetic viscosity of liquid
θ	=	impingement angle
θ_N	=	angle along the concave wall surface
ϕ	=	coordinate in the azimuthal direction on the solid wall
ω	=	radius of curvature of the streamline along the concave wall surface at ξ
ξ	=	radial distance from the stagnation point

Subscripts

ϕ	=	value at $\phi = \phi$
0	=	value at the point at which the laminar boundary layer reaches the liquid film surface

Superscript

*	=	nondimensional value

Introduction

THE phenomena of a liquid jet impinging on a solid wall and the generation of a liquid film on the wall are observed in the wall impingement-type injector and an internal engine. In these cases, the film thickness on the solid wall is an important factor with respect to the spray, combustion, and emission characteristics. In a previous paper [1], the authors theoretically analyzed the film flow on the flat wall and deduced the equations that predict the film thickness and film velocity. The predictions of the film thickness were compared with film thickness measurements, and the validity of the theoretical analysis was verified.

In contrast, in internal engines, the fuel jet generally impinges on a curved wall rather than on a flat wall. In the case of a wall impingement-type injector, it becomes possible to control the spray configuration by impinging a liquid jet on the curved wall, and so the design of the injector becomes more flexible.

Compared with the liquid flow on the flat wall, few studies have examined the liquid flow on the curved wall. In addition, there are several unknown characteristics concerning the film flow on the curved wall. In particular, the effects of the Taylor–Goertler vortex [2], which is generated in the boundary layer of a fluid flowing over a concave wall, on the liquid film thickness are unknown. In the present paper, the theoretical analysis of the liquid film flowing over the flat wall was extended to the film flow over the concave wall. Measurements of the film thickness on the concave wall were performed by the contact needle method in the range of the Goertler number at which the Taylor–Goertler vortex may be generated.

Experimental Apparatus and Conditions

Figure 1 shows the experimental apparatus used in the film thickness measurements. Liquid is pressurized in the water tank by the high-pressure air from the compressor and is supplied to the liquid nozzle through the flow meter and needle valve. The liquid nozzle is made of stainless steel and has an inner diameter of 0.5 mm and a length of 30 mm. The liquid nozzle can be rotated around the axis perpendicular to the page. The distance between the liquid

Received 7 September 2006; revision received 15 November 2006; accepted for publication 15 November 2006.

*Professor, Faculty of Science and Technology; tina@cc.hirosaki-u.ac.jp. Senior Member AIAA.
†Graduate Student, Faculty of Science and Technology.
‡Associate Professor, Faculty of Science and Technology.

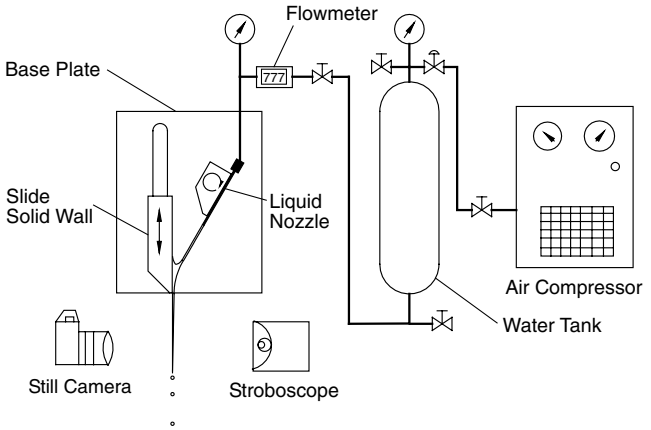

Fig. 1 Experimental apparatus.

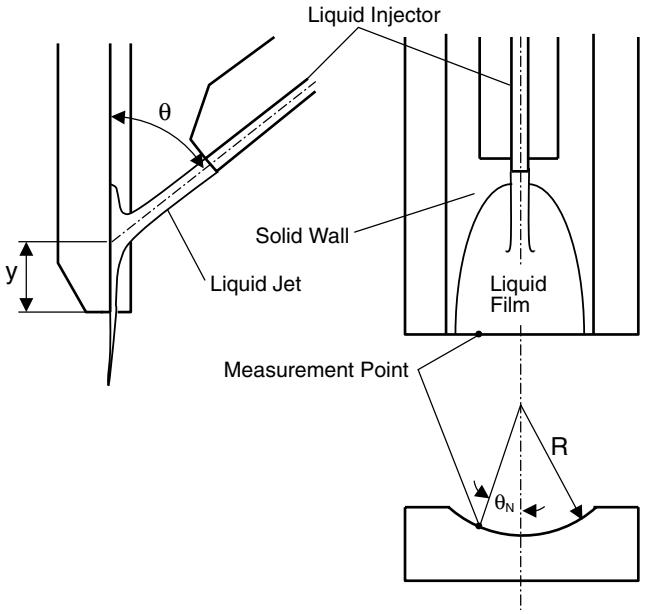

Fig. 2 Details of experimental setup.

nozzle exit and the impingement point on the solid wall was fixed at 10 mm. The impingement plate can be moved upward and downward, and the distance between the impingement point and the wall edge is adjustable.

The details of the impingement plate are shown in Fig. 2. The plate is made of brass, and its concave wall surface provides a cylindrical surface. The concave wall surface was polished by no. 1500 emery paper and polishing powder. The liquid film thickness on the concave wall was measured by the contact needle method [3]. The contact needle can be rotated around the center axis of the cylindrical wall surface. In the present study, the experiments were performed for the case that the center axes of the liquid nozzle and the cylindrical concave wall lie in the same plane, as shown in Fig. 2.

Tap water was used as the injection liquid. The experimental conditions are shown in Table 1. The positioning accuracy of a contact needle probe is 1 μm. However, the waves on a liquid film surface seem to affect the measurement of a film thickness. At the present stage, it is difficult to show the accuracy of the present method of film thickness measurement, because the exact thickness of the wavy liquid film is unknown due to the lack of the perfect measurement method. In the comparisons between the measurement by the contact needle method and the theoretical analysis in the case of normal impingement and low jet Reynolds number, the discrepancies were less than 15 μm, except for a hydraulic jump region [1]. In the case of normal impingement and low jet Reynolds number, it was made clear that the theoretical analysis estimates the film thickness very well [4]. Because the fluctuation width of a liquid film thickness in the case of high Reynolds number, such as the present experimental condition, seems to be smaller than that in the case of low Reynolds number, the effect of the waves on the liquid film surface on the measurement of the film thickness seems to be smaller in the present case, compared with the case of low Reynolds number. So, the measurement accuracy of a film thickness is roughly estimated to be less than 20 μm.

Table 1 Experimental conditions

Injection liquid	Tap water
Distance between impingement point and nozzle tip	10 mm
Nozzle diameter	0.5 mm
Radius of curvature of cylindrical concave wall, R	20–40 mm
Distance between measurement point and center axis, y	2–6 mm
Impingement angle	30–60 deg
Jet Reynolds number	3873–8134

Theoretical Analysis of Liquid Film Flow on the Concave Wall Surface

Based on the theoretical analysis of the liquid film flow on the flat solid wall [1], the liquid film flow on the cylindrical concave wall was analyzed theoretically. Before the theoretical analysis, the following assumptions were made:

1) The liquid flow is two-dimensional.

2) The liquid impinging on the solid wall spreads radially from the stagnation point.

3) The velocity distribution across the liquid jet is uniform, and the liquid flow in the liquid film on the solid wall is laminar.

4) On the solid wall, the laminar boundary layer in the liquid film develops from the stagnation point.

5) The velocity distribution across the laminar boundary layer can be approximated by the following quartic equation, which was reported by Ishigai et al. [5]:

$$u_\phi = U_\phi(2\eta - 2\eta^3 + \eta^4) \tag{1}$$

6) The liquid flowing at a minute angle $d\alpha$ in the liquid jet flows at a minute angle $d\phi$ in the liquid film, as shown in Fig. 3, in which the following geometric relationship of Rubel [6] exists between α, ϕ, and θ:

$$\tan\phi = \sin\theta \cdot \tan\alpha \tag{2}$$

7) In the case of the oblique impingement of a liquid jet on the solid wall, the centerline of the jet is not consistent with a streamline passing the stagnation point on the wall, as shown in Fig. 3. The distance between these two lines is expressed by the following equation [7]:

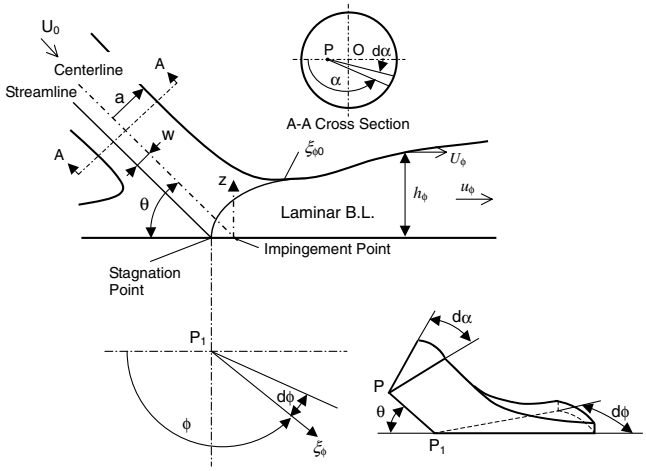

Fig. 3 Symbols and coordinate system employed in theoretical analysis of liquid film flow.

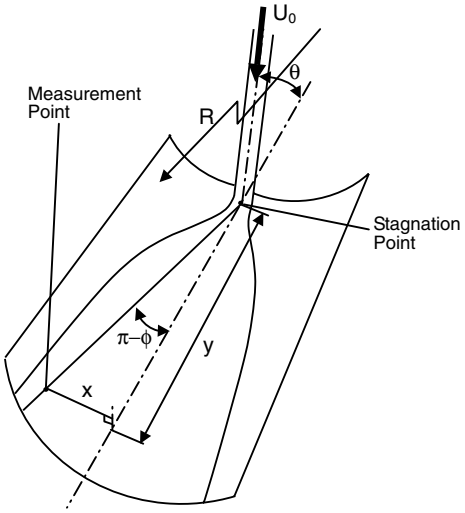

Fig. 4 Coordinate system.

$$w = a\cos\theta \tag{3}$$

8) The effect of the airflow on the liquid film and that of the gravity on the film behavior can be ignored.

9) The effect of the centrifugal force on the liquid flow can be ignored.

10) The effect of the Taylor–Goertler vortex on the liquid flow can be ignored.

The coordinate system used in the present analysis is shown in Figs. 4 and 5. Figure 6 shows the cross-sectional plane that obliquely cuts a cylinder with a plane including a water streamline from an impingement point and a perpendicular line at an impingement point. The liquid spreading radially in the direction of ϕ from the stagnation point flows along the circumference of an ellipse, as shown in Fig. 6. The trajectory of the liquid is given by the following equation:

$$\frac{X^2}{(R/\sin\phi)^2} + \frac{Y^2}{R^2} = 1 \tag{4}$$

On the other hand, the following equations are obtained based on Figs. 5 and 6:

$$X = \frac{x}{\sin\phi} = -\frac{y}{\cos\phi} \tag{5}$$

$$x = R\sin\theta_N \tag{6}$$

From Eq. (4), the following equation is derived:

$$Y^2 = R^2 - (X\sin\phi)^2 \tag{7}$$

Differentiating the preceding equation by X deduces the following equation:

$$\frac{dY}{dX} = -\frac{X}{Y}\sin^2\phi \tag{8}$$

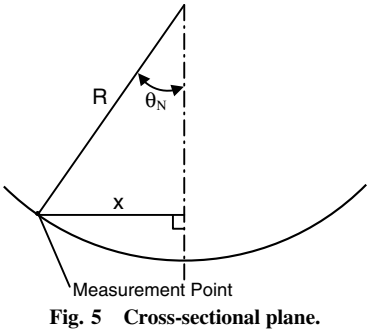

Fig. 5 Cross-sectional plane.

$$\frac{d^2Y}{dX^2} = -\frac{\sin^2\phi}{Y} + \frac{X}{Y^2}\sin^2\phi\frac{dY}{dX} = -\frac{\sin^2\phi}{Y} - \frac{X^2}{Y^3}\sin^4\phi \tag{9}$$

From Eqs. (5) and (6) the following equation is derived:

$$\tan\phi = -\frac{R\sin\theta_N}{y} \tag{10}$$

As shown in Fig. 6, the distance from the stagnation point to the measurement point along the concave wall surface is given by the following equation:

$$\xi_\phi = \int_0^X \sqrt{1 + \left(\frac{dY}{dX}\right)^2}\,dX = \int_0^{-\frac{y}{\cos\phi}} \sqrt{1 + \frac{X^2\sin^4\phi}{Y^2}}\,dX$$
$$= \int_0^{-\frac{y}{\cos\phi}} \sqrt{1 + \frac{X^2\sin^4\phi}{R^2 - X^2\sin^2\phi}}\,dX \tag{11}$$

On the other hand, a radius of curvature of the streamline along the concave wall surface is given by the following equation:

$$\omega_\phi = \frac{\{1 + (\frac{dY}{dX})^2\}^{3/2}}{|\frac{d^2Y}{dX^2}|} = \frac{(X^2\sin^4\phi + Y^2)^{3/2}}{\sin^2\phi(X^2\sin^2\phi + Y^2)} = \frac{(R^2 - y^2\sin^2\phi)^{3/2}}{R^2\sin^2\phi} \tag{12}$$

The liquid film flow on a wall surface was analyzed theoretically using the velocity distribution in a boundary layer proposed by Ishigai et al. [5] and a momentum equation of the laminar boundary layer. The details of the theoretical analysis are shown in [1]. The liquid film thickness at ϕ and ξ_ϕ is given as follows, according to the location at which the laminar boundary layer reaches the liquid film surface, as shown in Fig. 3, in which replacing ξ_ϕ and ξ_ϕ^* in the following equations by r_ϕ and r_ϕ^*, respectively, gives the same equations as those given in [1].

1) In the case of $\xi_\phi \le \xi_{\phi 0}$,

$$h_\phi^* = \frac{1}{2\xi_\phi^*}A\cdot B^2 + 1.79\sqrt{\xi_\phi^*} \tag{13}$$

where

$$h_\phi^* = \frac{h_\phi}{a}Re^{1/3} \tag{14}$$

$$\xi_\phi^* = \frac{\xi_\phi}{a}\cdot\frac{1}{Re^{1/3}} \tag{15}$$

$$Re = \frac{Q}{a\nu} \tag{16}$$

The continuity condition at $\xi_\phi = \xi_{\phi 0}$ and assumption (6) can be used to derive the following equation:

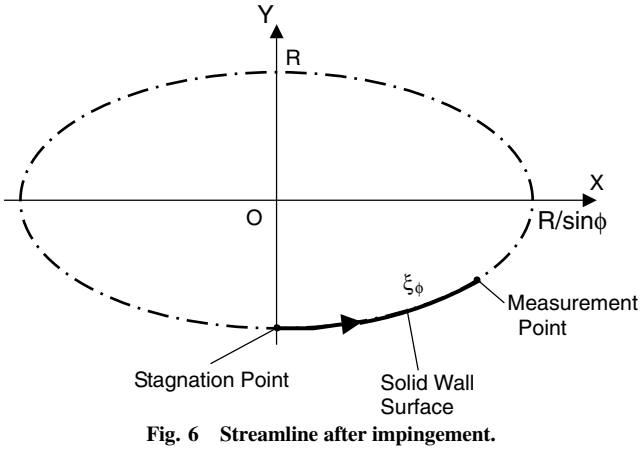

Fig. 6 Streamline after impingement.

$$\xi^*_{\phi 0} = \frac{\xi_{\phi 0}}{a} \cdot \frac{1}{Re^{1/3}} = \frac{0.564}{(4\pi)^{1/3}} A^{2/3} B^{4/3} \tag{17}$$

where

$$A = \frac{\sin\theta}{\sin^2\phi + \cos^2\phi \cdot \sin^2\theta} \tag{18}$$

$$B = \pm\cos\theta \sqrt{\frac{\sin^2\theta}{\tan^2\phi + \sin^2\theta}} + \sqrt{1 - \frac{\cos^2\theta \cdot \tan^2\phi}{\tan^2\phi + \sin^2\theta}} \tag{19}$$

where the sign of the first term on the right-hand side of Eq. (19) is negative when $0 \le \alpha < 90$ deg and positive when $90 \le \alpha < 180$ deg.

2) In the case of $\xi_\phi > \xi_{\phi 0}$,

$$h^*_\phi = \frac{0.642}{\xi^*_\phi} A \cdot B^2 + \frac{5.03 \xi^{*2}_\phi}{A \cdot B^2} \tag{20}$$

To calculate the liquid film thickness at y and θ_N, we first calculate ϕ from Eq. (10) and then calculate ξ_ϕ numerically from Eq. (11) using Simpson's rule. Next, we calculate $\xi_{\phi 0}$ from Eq. (17) and then calculate h_ϕ from Eqs. (13) and (14). Equations (14) and (20) are used to determine the film thickness after the boundary layer reaches the surface.

When the fluid flows along the concave wall, a Taylor–Goertler vortex may be generated in the boundary layer, because the boundary layer becomes unstable due to the centrifugal force [2]. The nondimensional Goertler number is known as the index that determines the occurrence of the Taylor–Goertler vortex. The critical nondimensional Goertler number at which the Taylor–Goertler vortex occurs is between 6 and 9 and depends on the turbulent intensity, for which the nondimensional Goertler number is defined by the following equation:

$$G = \frac{U_\phi \cdot \delta_{2\phi}}{\nu} \sqrt{\frac{\delta_{2\phi}}{\omega_\phi}} \tag{21}$$

Because in the region far from the impingement point, the laminar boundary layer reaches a liquid film surface, $\delta_{2\phi}$ is derived as follows from the aforementioned velocity distribution in the boundary layer:

$$\begin{aligned}\delta_{2\phi} &= \frac{1}{U^2_\phi}\int_0^{\delta_\phi} u_\phi (U_\phi - u_\phi)\,\mathrm{d}z = \frac{1}{U^2_\phi}\int_0^1 U^2_\phi (2\eta - 2\eta^3 \\ &\quad + \eta^4)(1 - 2\eta + 2\eta^3 - \eta^4)\delta_\phi\,\mathrm{d}\eta = \delta_\phi \int_\phi^1 (2\eta - 2\eta^3 \\ &\quad + \eta^4)(1 - 2\eta + 2\eta^3 - \eta^4)\,\mathrm{d}\eta = 0.784\delta_\phi\end{aligned} \tag{22}$$

where U_ϕ and δ_ϕ are given as follows, according to ξ_ϕ:

1) In the case of $\xi_\phi \le \xi_{\phi 0}$,

$$U_\phi = U_0 \tag{23}$$

$$\delta^*_\phi = 5.97\sqrt{\xi^*_\phi} \tag{24}$$

where

$$\delta^*_\phi = \frac{\delta_\phi}{a} Re^{1/3} \tag{25}$$

Replacing ξ^*_ϕ in Eq. (24) by r^*_ϕ gives Eq. (5) in [1].

2) In the case of $\xi_\phi > \xi_{\phi 0}$,

$$U_\phi = \frac{U_0}{0.899 + 7.04 A^{-2} B^{-4} \xi^{*3}_\phi} \tag{26}$$

$$\delta^*_\phi = h^*_\phi \tag{27}$$

Replacing ξ^*_ϕ in Eq. (26) by r^*_ϕ gives Eq. (15) in [1].

Experimental Results and Discussions

Effect of Radius of Curvature of the Concave Wall Surface

Figure 7 shows the effect of the radius of curvature on the film thickness distribution. The measurement point is 3 mm downstream of the impingement point and the impingement angle is 30 deg. The Reynolds number is 5420. The curved lines in the figure show the film thickness predicted by the theoretical analysis. The film thickness has a peak at the center. As the angle θ_N increases, the film thickness first decreases and then increases. The maximum and minimum film thicknesses are invariable with respect to the radius of curvature. However, θ_N at the minimum film thickness decreases as the radius of curvature increases. The tendency of the calculated film thickness with respect to θ_N agrees well with that of the measurements. The quantitative discrepancies in the film thickness between the predictions and measurements are approximately 10 μm. In the center region, the predictions underestimate the film thickness regardless of the radius of curvature. This discrepancy in the center region appears to be due to the assumptions made before the theoretical analysis of the film flow. In assumption (6), it is assumed that the liquid flowing at a minute angle $\mathrm{d}\alpha$ in the liquid jet flows at a minute angle $\mathrm{d}\phi$ in the liquid film. However, this assumption may not be realistic in the vicinity of both the symmetry axis of the film flow and the impingement point. Indeed, the liquid flow in the vicinity of both the symmetry axis and the impingement point may be three-dimensional because the liquid film is thick and the liquid inertia is large.

The range of θ_N in which the measurement was carried out was limited. The film thickness increases sharply at the periphery because of the hydraulic jump. In the present analysis, the hydraulic jump is not taken into account. Therefore, the measurements were restricted to the range from the center to the point at which the hydraulic jump occurs. Figures 8 and 9 show the location at which the hydraulic jump occurs. In Fig. 8, the Reynolds number is 5420 and the radius of a concave wall is 30 mm. As the impingement angle increases, the location of a hydraulic jump spreads to the periphery. In Fig. 9, the radius of a concave wall is 30 mm and the impingement angle is 30 deg. As the Reynolds number increases, the location spreads slightly. In both cases, the location lines of a hydraulic jump are not bilateral symmetry. This is due to the delicate condition differences of the wall surface. The location of a hydraulic jump is greatly influenced by the inclination and roughness of a wall surface, the contact angle between the liquid and the wall surface, etc., as well as the impingement angle and the Reynolds number. So, it is difficult to estimate the location of the hydraulic jump under the different conditions. In the present paper, the theoretical analysis of a liquid film flow is limited to the upstream region of the location at which the hydraulic jump occurs.

Figure 10 shows the effect of the radius on the film thickness distribution at $y = 6$ mm. The other experimental conditions are the same as those in Fig. 7. The peak of the film thickness is smaller and the minimum film thickness is larger than those in Fig. 7. In addition, the film thickness distribution becomes flatter compared with that in Fig. 7.

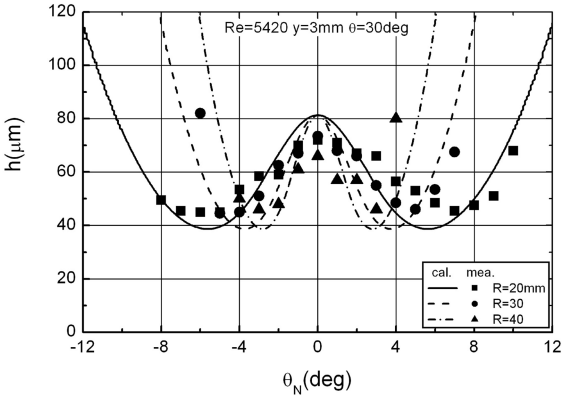

Fig. 7 Effect of the radius of curvature at $y = 3$ mm.

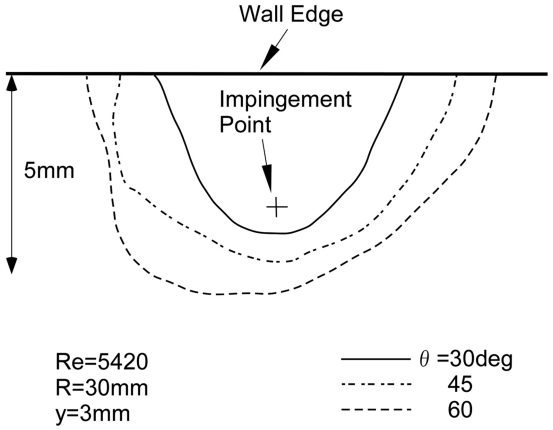

Fig. 8 Effect of the impingement angle on the location of the hydraulic jump.

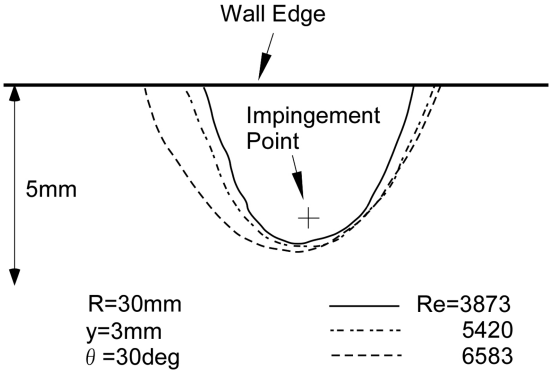

Fig. 9 Effect of the Reynolds number on the location of the hydraulic jump.

Figure 11 shows the effects of the radius of curvature of the streamline on the film thickness distribution at $\theta = 60$ deg. The other experimental conditions are the same as those in Fig. 7. In the case of $\theta = 60$ deg, the changes in film thickness in the center region are small and increase rapidly at the periphery. The predictions agree well with the measurements.

The standard experimental conditions of the figures shown next are indicated in Table 2, unless otherwise stated.

Effect of Impingement Angle

Figure 12 shows the effect of the impingement angle on the film thickness distribution. The experimental conditions are the preceding standard experimental conditions, except for the impingement angle. As the impingement angle increases, the film thickness in the center region decreases. On the other hand, the minimum film thickness is approximately constant, irrespective of the impingement angle. Consequently, the film thickness distribution becomes flat with increasing the impingement angle. Quantitatively, the predictions agree well with the measurements, except in the center region at $\theta = 30$ deg.

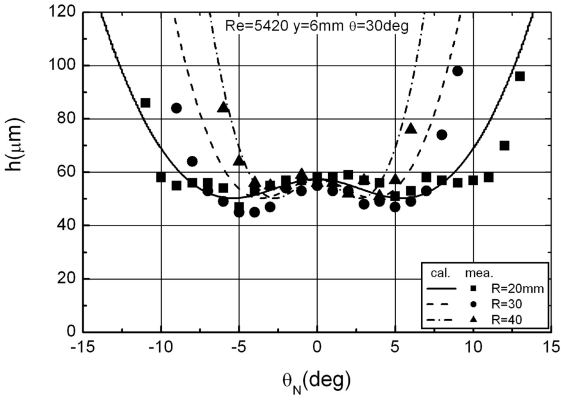

Fig. 10 Effect of the radius of curvature at $y = 6$ mm.

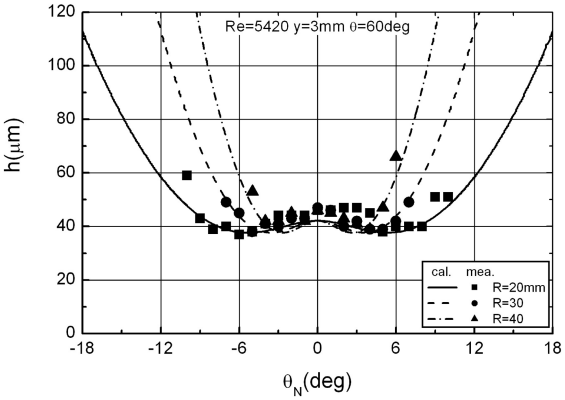

Fig. 11 Effect of the radius of curvature at $\theta = 60$ deg.

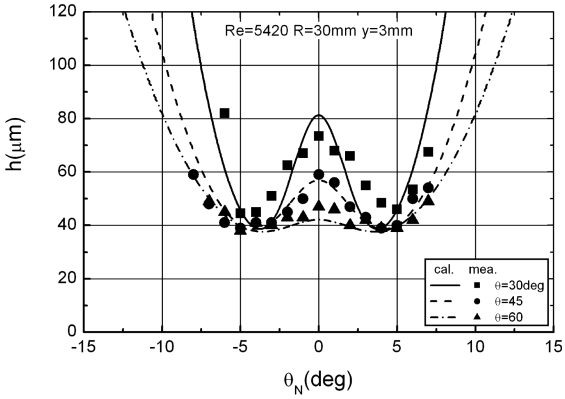

Fig. 12 Effect of the impingement angle.

Effect of Distance Between Measurement and Impingement Points

Figure 13 shows the effect of the distance between the measurement and impingement points on the film thickness distribution. The experimental conditions are the preceding standard experimental conditions, except for the distance between the measurement and impingement points. As this distance increases, the film thickness in the center region decreases and the minimum film thickness increases. Consequently, the film thickness distribution becomes flat with increasing distance. Quantitatively, the predictions agree well with the measurements, except in the center region at $y = 2$ mm. The discrepancy between the predictions and measurements in the center region at $y = 2$ mm is due to the invalidity of the preceding assumption (6).

Effect of Reynolds Number

Figure 14 shows the effect of the Reynolds number on the film thickness distribution. The experimental conditions are the standard experimental conditions, except for the Reynolds number. As the Reynolds number increases, both the peak film thickness at the center and the minimum film thickness decrease. The angle θ_N at which the film thickness has a minimum value increases more or less with

Table 2 Standard experimental conditions

Radius of curvature of cylindrical concave wall, R	30 mm
Distance between measurement point and center axis, y	3 mm
Impingement angle	30 deg
Jet Reynolds number	5420

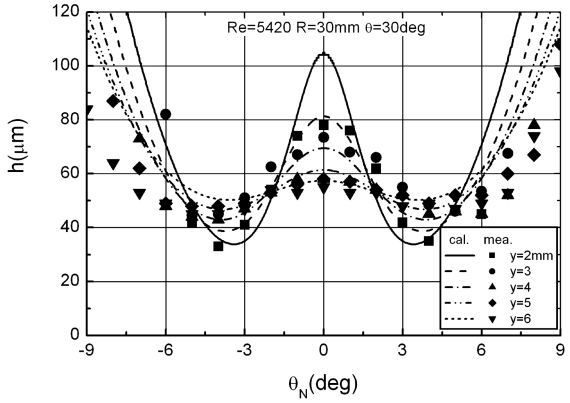

Fig. 13 Effect of the distance between impingement and the measurement point.

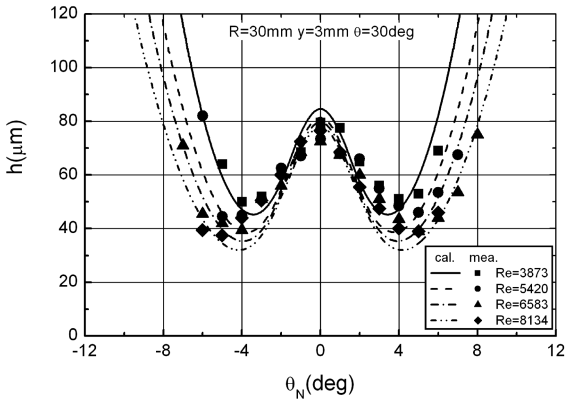

Fig. 14 Effect of the Reynolds number.

increasing Reynolds number. Quantitatively, the predictions agree well with the measurements, except in the center region.

For the present experimental setup, the backward liquid film flow gives rise to a hydraulic jump and forms a thick rim. The liquid flows downstream inside the thick rim and then it issues from a wall edge, taking the form of a thick ligament. The thick rim is one of the important factors for the spray characteristics of a wall impingement-type injector and other applications. However, as aforementioned, the estimation of a location at which the hydraulic jump occurs is difficult at the present stage. So, the theoretical and experimental investigations about the hydraulic jump will be the next step of our study.

Effect of the Taylor–Goertler Vortex on the Film Thickness Distribution

Figure 15 shows the distribution of the maximum Goertler number along the streamline from the impingement point to the measurement point. The experimental conditions are standard, except for the Reynolds number. Because the radius of curvature changes along the streamline, the Goertler number also changes along the streamline. The maximum Goertler number exceeds six, at which point the Taylor–Goertler vortex may occur, except when θ_N is less than 2 deg. In the center region, the Goertler number is smaller than in other regions because of the larger radius of curvature.

As shown in Fig. 15, the Taylor–Goertler vortex may be generated in all but the center region. However, the film thicknesses predicted by the theoretical analysis under the assumption that the effect of the Taylor–Goertler vortex on the liquid flow can be ignored are approximately coincident with the measurements. This implies either that the Taylor–Goertler vortex does not occur, despite the

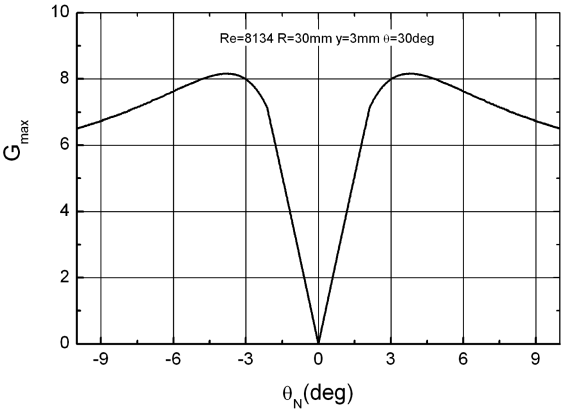

Fig. 15 Maximum Goertler number along the streamline.

large Goertler number, or that the Taylor–Goertler vortex does not affect the film thickness even if it occurs. However, these conclusions are applicable to the present narrow ranges of the experimental conditions. To clarify the effect of the Taylor–Goertler vortex, further studies examining wide ranges of experimental conditions for the liquid film flowing over the concave wall should be conducted.

Conclusions

The theoretical analysis of the liquid film flowing over the concave wall was deduced based on the theory of the film flow on the flat wall. The thickness of the liquid film on the concave wall was measured over a wide range of Goertler numbers, including the region in which the Taylor–Goertler vortex may occur, and the obtained measurements were compared with those obtained through theoretical analysis. The predictions of the film thickness on the concave wall surface obtained by theoretical analysis agree well with the measurements, despite the use of several assumptions, except in the vicinities of the symmetry axis and the impingement point. In the range of the present experimental conditions, the Taylor–Goertler vortex has a negligibly small effect on the film thickness.

In the present theoretical analysis, the effect of a hydraulic jump was neglected. The detailed investigation of the hydraulic jump is left to the future study.

References

[1] Inamura, T., Yanaoka, H. and Tomoda, T., "Prediction of Mean Droplet Size of Sprays Issued from Wall Impingement Injector," *AIAA Journal*, Vol. 42, No. 3, 2004, pp. 614–621.

[2] Schlichting, H., *Boundary-Layer Theory*, McGraw–Hill, New York, 1968, pp. 500–509.

[3] Inamura, T., and Tomoda, T., "Characteristics of Sprays Through a Wall Impingement Injector," *Atomization and Sprays*, Vol. 14, No. 4, 2004, pp. 375–395.

[4] Azuma, T., and Hoshino, T., "The Radial Flow of a Thin Liquid Film (2nd Report)," *Transactions of the Japan Society of Mechanical Engineers (Series B)*, Vol. 50, No. 452, 1984, pp. 982–989 (in Japanese).

[5] Ishigai, K., Nakanishi, S., Mizuno, M. and Imamura, T., "Heat Transfer by Impingement of Round Water Jet," *Transactions of the Japan Society of Mechanical Engineers*, Vol. 42, No. 357, 1976, pp. 1502–1510 (in Japanese).

[6] Rubel, A., "Computations of the Oblique Impingement of Round Jets upon a Plane Wall," *AIAA Journal*, Vol. 19, No. 7, 1981, pp. 863–871.

[7] Hasson, D., and Peck, R. E., "Thickness Distribution in a Sheet Formed by Impinging Jets," *AIChE Journal*, Vol. 10, No. 5, 1964, pp. 752–754.

D. Talley
Associate Editor